Proceedings of FEDSM2018
5th Joint US-European Fluids Engineering Summer Conference
July 15-20, 2018, Montreal, Quebec, Canada

FEDSM2018-83077

SMALL BUBBLES GENERATION WITH SWIRL BUBBLERS FOR SNS TARGET

C. Barbier **E. Dominguez-Ontiveros** **R. Sangrey**

Oak Ridge National Laboratory (UT-Batelle, LLC), Oak Ridge, TN 37831 USA

ABSTRACT

Oak Ridge National Laboratory's (ORNL) Spallation Neutron Source (SNS) uses a mercury target to generate neutrons. When the powerful 1.4 MW, 60Hz proton beam hits the target, a strong pressure wave propagates in the mercury and into the vessel wall due to the rapid temperature rise in mercury. These pressure waves induce cavitation damage on the target container and high stresses, which both limit the lifetime of the target. Since October 2017, helium gas has been injected into the mercury flow in order to mitigate the negative effects of pulse-induced pressure waves. The preliminary strain measurements suggest that gas injection is indeed efficient at mitigating the pressure wave. Tiny nozzles (8-micron diameter) at choked condition are used to generate small bubbles. The bubblers can theoretically inject a total mass flow rate of 0.75 SLPM. However, during operation the bubblers were capable of injecting only approximately 0.45 SLPM, which suggests that some of the nozzles may have become clogged. Since there is a strong desire to inject a larger quantity of gas in the target to, hopefully, mitigate even more the pressure wave, SNS has been looking at implementing swirl bubblers in the target, similar to the ones used in the Japan Proton Accelerator Research Complex (J-PARC) mercury target. In this paper, results with prototypical bubblers tested in water and mercury are presented. Bubblers were installed in prototypical targets and bubble size distributions were measured in both water and mercury. It was found that swirl bubblers can generate a large number of small bubbles, but some compromises were made to keep the pressure losses across them reasonable.

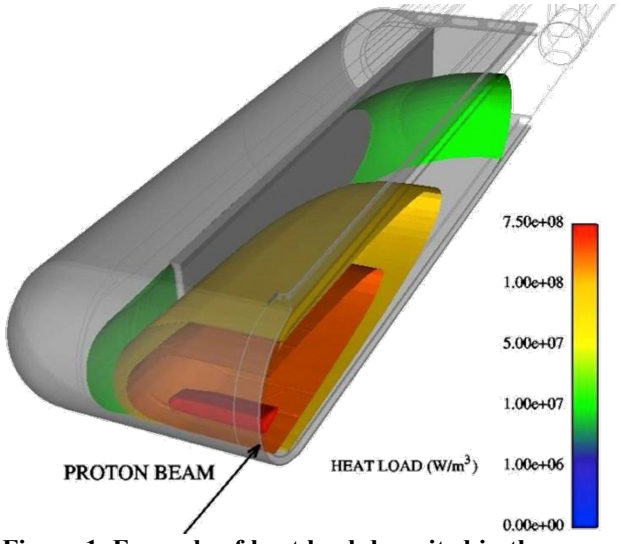

Figure 1. Example of heat load deposited in the mercury for a 1.4MW, 1GeV proton beam.

INTRODUCTION

The Spallation Neutron Source (SNS) is a research facility located in Oak Ridge, Tennessee (USA) that provides the most intense pulsed neutron beam in the world. A 1.4MW, 60 Hz beam proton hits the mercury target to knock (or spallate) neutrons out of it. Neutron moderators surround the target that convert the spallation

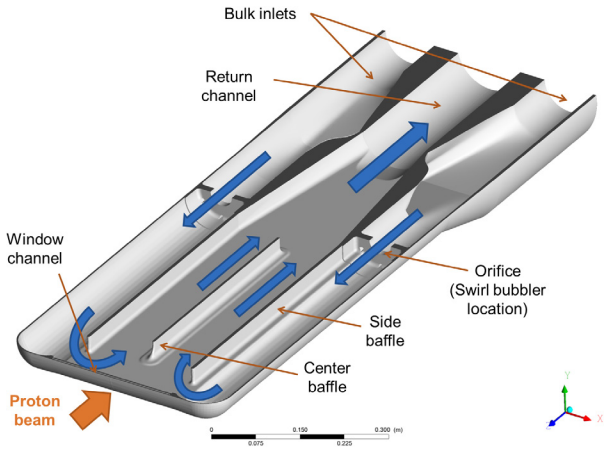

Figure 2. 3D cross-section view of the inside of the mercury target (without bubblers) and description of the mercury flow pattern.

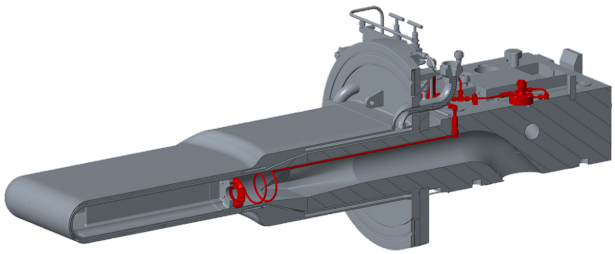

Figure 3. Implementation of gas injection in the SNS target. The gas injection hardware is shown in red.

neutrons into slow neutrons that are then distributed among several instruments for scientific research. The mercury is contained into a stainless steel vessel, and flows to remove the heat deposited by the proton beam. When the proton beam hits the liquid mercury target, an intense heat load (see Figure 1) is deposited into the mercury, which leads to a rapid rise in temperature (10^7 K/s). The sudden thermal expansion generates an intense pressure wave in the mercury that drives high cycle fatigue in the target vessel and cavitation of the mercury. The pressure field when the proton beam hit the target can be estimated with:

$$P = Q\,\frac{\beta K}{f \rho C_V}$$

where:

- P is the increase in pressure
- β the volumetric expansion coefficient
- f the beam pulse frequency
- ρ the mass density
- C_v the constant volume specific heat
- Q the volumetric power
- K the bulk modulus

Thus, for a heat load as shown in Figure 1, a corresponding peak pressure of ~35MPa in the mercury and ~14MPa in the stainless steel occur. The pressure wave reflection and rarefaction in the vessel lead to tension in mercury causing cavitation. SNS has been investigating mitigating the effects of pulse-induced pressure waves in mercury since 2001 [1]. One of the mitigation methods is the injection of small (less than 150μm diameter), non-condensable gas bubbles in mercury that can attenuate the pressure wave that drives cavitation and high cycle fatigue [2]. Gas injection in the mercury target was successfully implemented at SNS in October 2017. Small bubbles were generated using small orifices (8-micron diameter) located in the bulk inlet of the target (see Figure 2 and 3 for the setup and location of the bubbler in the target). More details on the flow pattern in the target can be found in [3].This bubbler has been investigated by SNS [4][5] and demonstrated its ability to generate bubbles less than 150 micron diameter. A high pressure supply is used (100 psig) such that the orifices are in choked-flow condition, and thus, injecting at a constant flow rate. The measured strain showed that a gas injection of 0.45 SLPM of helium can lead to strain reduction up to 63% (see Figure 4). The total mercury mass flow rate is about 975 LPM, and the pressure in the target is ~40psig. Thus, despite the very low injected volume fraction in the target, only 0.012%, considerable pressure wave mitigation was measured. Figure 5 and 6 show the response of a single sensor located at the tip of the target with and without gas injection, it can be observed that gas injection not only decreased the strain but also changed the vessel dynamic response to the pressure wave. Figure 7 shows the relation between the strain and the gas injection flow rate: the more the gas injection flow rate, the more the strain reduction. Thus, there is a strong desire in injecting more gas in the SNS target to mitigate the pressure wave even more and improve the target reliability and life span.

Although the small orifice bubbler is capable of generating the right bubble sizes to mitigate the pressure wave, it has several shortcomings:

- Fabrication difficulty: the nozzles need to be welded without being clogged.
- Unsteady gas injection: bubbler flow rate decreased during operation, indicating that some nozzles may have clogged during operation.

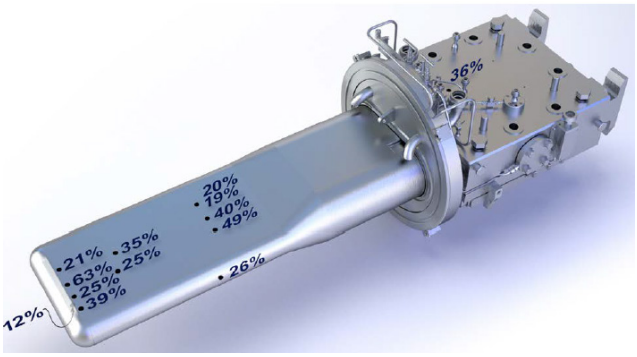

Figure 4. Target module with strain reduction percentage due to gas injection at up to 1.4MW at various sensor locations on the vessel.

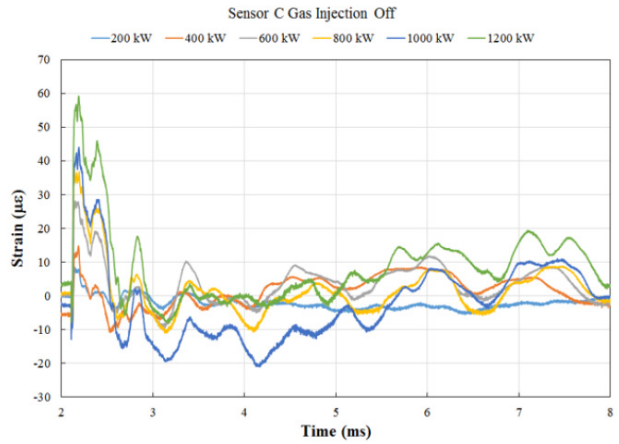

Figure 5. Strain measurements at the target's nose for several beam powers without gas injection (courtesy of W. Blokland and Y. Liu, SNS, ORNL).

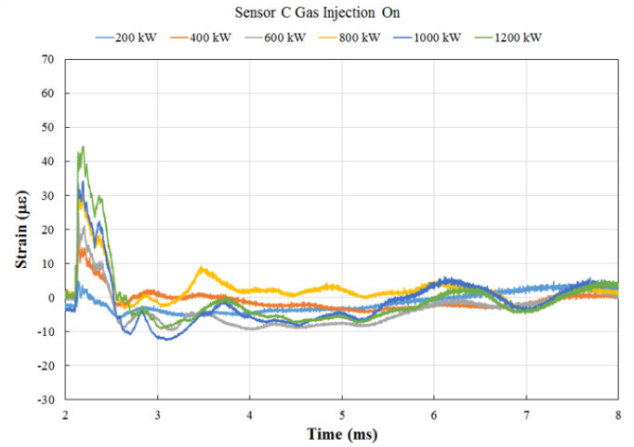

Figure 6. Strain measurements at the target's nose for several beam powers with gas injection (courtesy of W. Blokland and Y. Liu, SNS, ORNL).

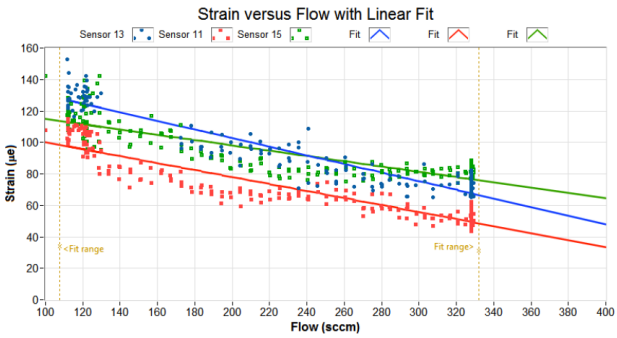

Figure 7. Peak strain measurements plotted versus the helium flow. Sensors are located ~0.5m away from the tip of the target (courtesy of W. Blokland and Y. Liu, SNS, ORNL).

- Cannot inject large quantity of gas: increasing the nozzle diameter would lead to larger bubbles, and pressure mitigation may not be as efficient.

Thus, SNS has been looking at implementing swirl bubblers [6], [7] in the target, similar to the ones used in the Japan Proton Accelerator Research Complex (J-PARC) mercury target. The present paper shows the latest investigation performed at ORNL on prototypical swirl bubbler. The swirl bubblers were designed specifically to satisfy the following requirements: (a) the pressure loss must be low enough to keep an acceptable mercury flow rate in the target; and (b) most of the bubbles generated must be less than 150 μm diameter. In the following, the swirl bubbler is described in detail and the SNS prototypical swirl bubbler is presented. Then bubble size distributions measured in water and mercury are presented, which demonstrate that a swirl bubbler is a possible solution to further mitigate the pressure wave in SNS target.

SWIRL BUBBLER

A schematic of a swirl bubbler is shown in Figure 8: a swirling flow is generated with fixed vanes and then accelerated through a constriction (venturi). Gas is injected at the center of the vanes, and is sheared by the swirling flow into bubbles. At the bubbler exit, the rounded edge causes the jet flow to attach itself to the wall (Coanda effect), which leads to additional bubble breakdown.

The characteristic bubble diameter d generated by the swirl bubbler can be estimated with [8]:

$$d = 1.26\left(\frac{\sigma^3}{\epsilon^2\rho^3}\right)$$

where σ is the surface tension, ρ the liquid density, and ϵ the visco dissipation. The dissipation rate can be estimated with:

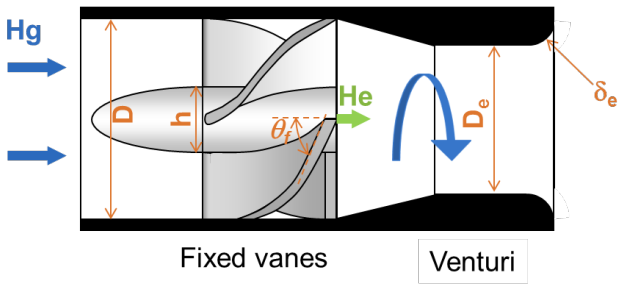

Figure 8. Schematic and characteristics dimensions of a swirl bubbler (courtesy of H. Kogawa).

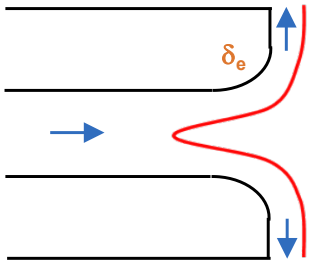

Figure 9. Coanda effect at the swirl bubbler exit.

$$\epsilon = D_e^2 f_e^3$$

where D_e is the diameter of the venturi (see Figure 8) and f_e is the swirl frequency at the bubbler outlet ($2V_e tan\theta_f / D_e$).

The Coanda effect occurs if (a) the swirl is strong enough that some suction occurs in the center of the channel; and (b) the exit surface are "rounded" enough that the wall jet remains attached (see Figure 8). To get some backflow in the bubbler (see red profile in Figure 9), the swirl number S_e (ratio of the azimuthal over the axial velocity) must be larger than two (subcritical swirling flow). Since the vortex flow is created only by the vanes geometry, it imposes that θ_f must be larger or equal than 60°. Next, using the same argument presented by Bradshaw [9], the flow remains attached on the curved surface if the pressure at the wall remains lower than the ambient pressure:

$$\rho U_{axial}^2 \frac{D_e/2}{\delta_e} \leq \rho U_{azimuthal}^2$$

Or:

$$\delta_e \geq \frac{D_e}{2S_e^2}$$

The pressure drop across the bubbler can be roughly estimated using the correlations presented in [10] from our colleagues at J-PARC. Similar to [10], an array of several swirl bubblers with alternative swirl directions was chosen (see Figure 10). The swirl bubblers are located in the bulk inlets of the target, where there was originally a flow restriction ("orifice" in Figure 2). In the bulk inlet, the mercury flow is about 1 m/s, and the hydraulic diameter is about 0.1m. Bubblers were 3D printed and the quick fabrication allowed us to try several configurations. Only the final bubbler configuration is presented here and its characteristic dimensions are shown in Table 1. Compared to J-PARC swirl bubblers [11], additional holes were added in the bubbler to decrease the pressure loss. In addition, the center hole was found to be efficient to keep the vortices apart longer.

Table 1. Characteristic dimensions of the swirl bubbler.

$\boldsymbol{D}$	36 mm
$\boldsymbol{D_e}$	32 mm
$\boldsymbol{h}$	7.2 mm
$\boldsymbol{\theta_f}$	65°
$\boldsymbol{\delta_e}$	4 mm

EXPERIMENTS IN WATER

The same test loop presented in [3] was used. A water loop with an acrylic target mockup target at the scale 1:1 was fabricated. The outside surfaces are flat to avoid optical distortion making bubble size measurement easier.

The flow resistance coefficient was measured and found to be 30. A shadowgraphy technique was used to determine the bubble size distribution. A Manta G145C IRC camera from Allied Vision Technologies (1,388×1,038 pixels, 30 fps) with a telecentric lens (variable zoom 0.75X to 4.5X) were used. A resolution of 31.8 μm/px was achieved with a depth of field of 0.5 to 1.5 mm. The image analysis was performed with ImageJ [12]. The image analysis was performed on a series of 100 pictures and consisted of the following steps:

1. Crop the image to remove the shadow created by the telecentric lens.
2. Use a Canny edge detector [13] to detect the edge of the bubbles.
3. Perform some simple binary operations (dilate, close, fill, erode) to make the bubble inside black.
4. Use the particle analyzer in ImageJ to determine the cross-section area of each bubbles. Discard the bubbles that are too big or not circular enough (generally a bad bubble detection).
5. Determine the bubble diameter based on its cross-section area.

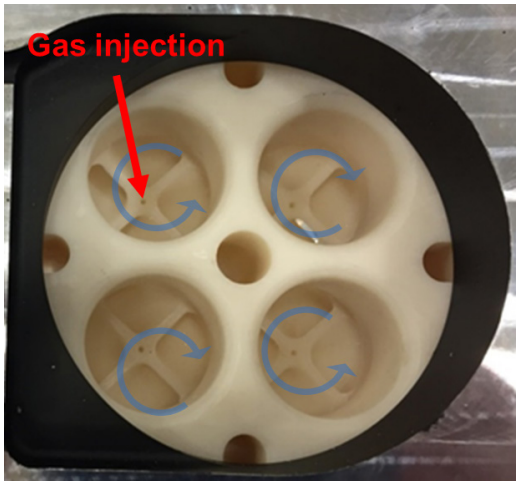

Figure 10. Picture of the back of swirl bubbler tested at SNS in a prototypical water target.

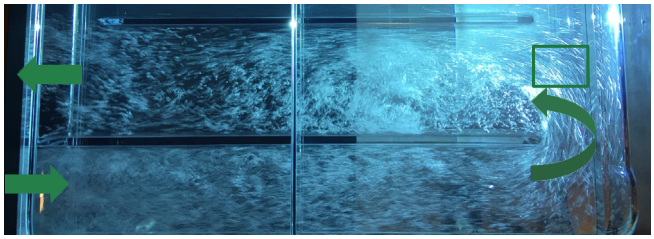

Figure 11. Picture of the bubbles generated with the swirl bubbler in water (V_{bulk} = 1.0 m/s, void fraction = 0.1%). The rectangle indicates where the bubble diameters were measured.

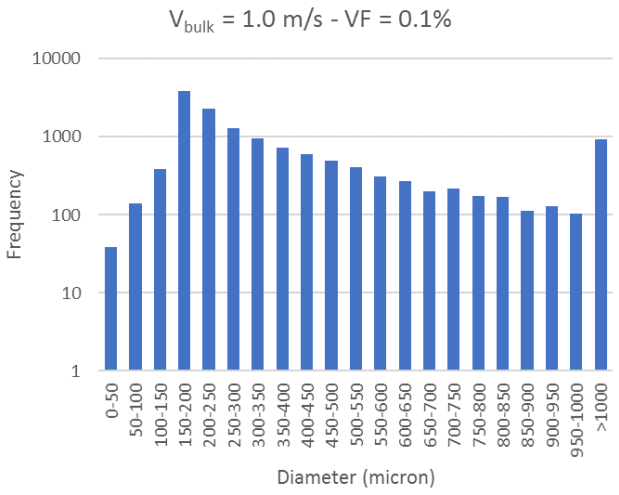

Figure 12. Bubble Size Distribution (BSD) determined at the location indicated in Figure 10 (V_{bulk}=0.1 m/s, VF = 0.1%).

Figure 11 shows the bubbly flow with an average bulk velocity V_{bulk} of 1.0 m/s and a volumetric void fraction of 0.1%. Measurements with higher void fractions were not possible because of the limitation of the shadowgraphy technique: high contrast pictures could not be obtained because the background was too dark due to the presence of more bubbles.

It was observed that bubble coalescence occurred in the return channel and that the bubbles were visibly larger in the return than just downstream of the bubbler (see Figure 11). When the bubbles are larger, they rise faster to the top of the channel and most of the bubbles were located at the top middle half of the pipe downstream of the target (not shown).

Bubble size distribution was determined at the tip of the target, in the middle of the height where the beam proton hits (see Figure 11 for the exact location). The most frequent bubble diameter was 150-200 μm, which matches with the 177 μm predicted by the theory. Based on the theory, the bubbles in mercury with the exact same geometry are expected to be of the order of 120 μm. The Coanda effect was observed at the exit of the bubbler: the gas vortex line is swirling along the bubbler exit and breaking down in small bubbles. Since the results with prototype were satisfying, a similar prototype made of stainless steel was built for testing in mercury.

EXPERIMENTS IN MERCURY

Experiments in mercury were performed at the Target Test Facility (TTF), a full-scale prototypical mercury loop (see Figure 13 and 14). 3D printed stainless steel swirl bubblers (see Figure 15) were installed in the prototypical target, with the same dimensions that the one used in water. To measure the BSD, a transient sample and settle technique was used as presented in [5]: a sample of the bubbly flow is extracted with a sampler tube, which is isolated using two valves. The sampled bubbly mercury sample is then at rest, and the bubbles rise to the top due to buoyancy force. A camera on the top records the bubbles hitting a glass window (see Figure 13 and 14). An example of a picture taken with the diagnostic sampler 100 seconds after closing the valves is shown in Figure 16. The resolution of the pictures was 2,560 × 1,920, resulting in a resolution of 4.4 μm/px. Similarly to the experiments in water, the bubble size is determined with ImageJ. Then several corrections are made to take into account the contact angle on the glass window and the pressure difference between the sampler and where the bubble were extracted. The overall factor correction for an average flow velocity of 1.1 m/s in the bulk inlet was 0.53. Thus, a measured 100 μm diameter bubble at the window corresponds to a 53 μm diameter bubble in the target. All

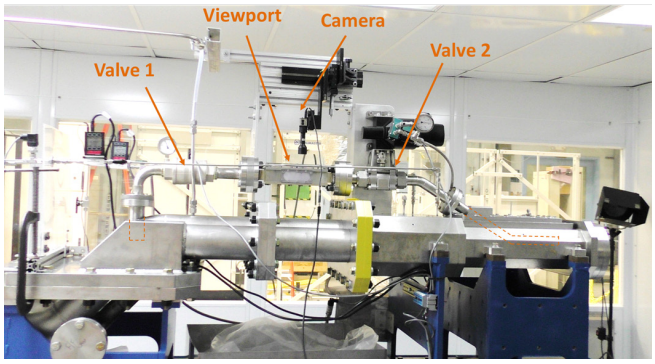

Figure 13. Target Test Facility with diagnostic sampler on the top.

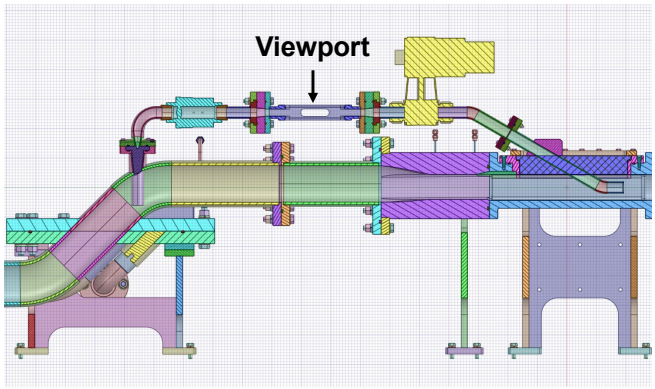

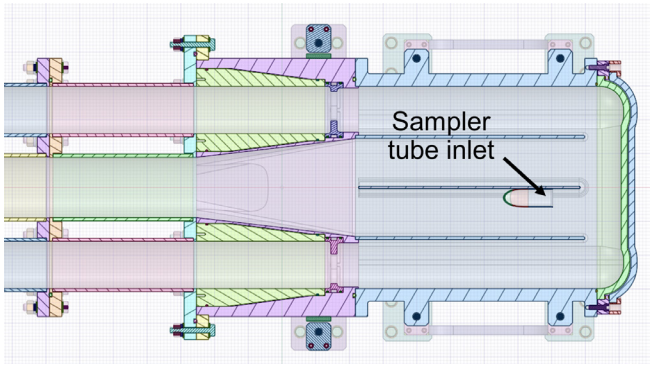

Figure 14. Cross-section side view (top) and top view (bottom) of the TTF target and its diagnostic sampler.

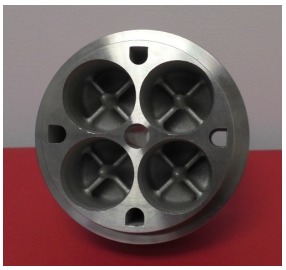

Figure 15. 3D printed stainless steel swirl bubbler.

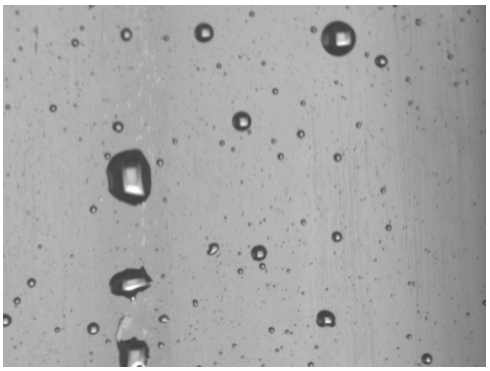

Figure 16. Example of picture taken with the diagnostic sampler. The picture height is 8.45 mm.

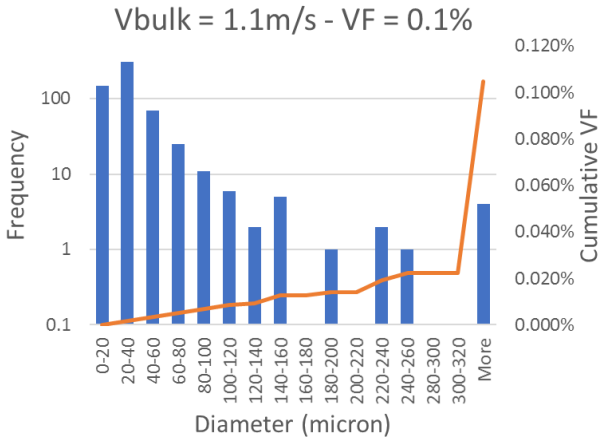

Figure 17. BSD and cumulative void fraction determined from Figure 15.

the bubble sizes presented here are corrected and are thus the estimated bubble size in the flow.

Measurements were performed with an averaged velocity V_{bulk} of 1.1m/s in the bulk flow. Slightly higher velocity than in water experiments was needed to get the sampler tube filled with mercury. With such bulk velocity, the theory predicts a bubble diameter of 106 μm.

the bubble sizes presented here are corrected and are thus the estimated bubble size in the flow.

The nose of the TTF target is made of acrylic and allows a first observation of the bubbles. Because of the curved shape of the nose, it is relatively difficult to measure the bubble size at that location. At least, it was observed that the bubbles were small and no large bubbles (>5 mm diameter) could be observed.

BSD measured with the diagnostic sampler is shown in Figure 17. The bubbles were much smaller than expected, with a peak in the 20-40 μm size. The cumulative fraction reached the expected void fraction 0.1%, and it can be seen how large bubbles have the most impact on the

cumulative fraction. In the BSD shown in Figure 16, only 4 bubbles have a diameter above 320 μm, and they contribute to most of the cumulative fraction. The bubble sizes measured were found much smaller than the expected 106 μm. It is possible that the sample taken is not representative of the bubbles generated by the swirl bubbler, and that somehow, only smaller bubbles are getting sampled while the larger are flowing above the sampler tube. Another possibility is that the bubbles are breaking up in even smaller size downstream of the bubbler due to the higher turbulence (the Reynolds number is ~10^6 in mercury whereas it was only 10^5 in water). According to [2], such small bubbles would be very efficient in mitigating the pressure wave.

Several measurements were performed (8 total) for different gas injection rate (up to 0.5% void fraction). For each gas injection rate, the BSD was similar to the one presented in Figure 17 which suggest that the BSD is not affected by the gas injection rate.

CONCLUSIONS

This study shows that the swirl bubbler investigated is a suitable bubbler for small bubble injection in the SNS target. Very good agreement with the theory was found for the experiments in water. However, much smaller bubbles were found in mercury, which may be due to the measurement technique or further bubble breakdown due to higher turbulence. According to the literature, the bubble size measured in mercury are small enough to significantly mitigate the pressure wave caused by the proton beam.

REFERENCES

[1] B. W. Riemer, M. W. Wendel, D. K. Felde, A. A. Abdou, and D. A. McClintock, "Status of R&D on mitigating the effects of pressure waves for the Spallation Neutron Source mercury target," *J. Nucl. Mater.*, vol. 431, no. 1–3, pp. 160–171, 2012.

[2] M. Futakawa *et al.*, "Mitigation Technologies for Damage Induced by Pressure Waves in High-Power Mercury Spallation Neutron Sources (II)—Bubbling Effect to Reduce Pressure Wave—," *J. Nucl. Sci. Technol.*, vol. 45, no. 10, pp. 1041–1048, 2008.

[3] C. Barbier and E. Dominguez-Ontiveros, "Improving Computational Fluid Dynamics Simulations for the Spallation Neutron Source Jet-Flow Target," in *ASME 2016 Fluids Engineering Division Summer Meeting collocated with the ASME 2016 Heat Transfer Summer Conference and the ASME 2016 14th International Conference on Nanochannels, Microchannels, and Minichannels*, 2016, p. V01AT03A011.

[4] M. Wendel, A. Abdou, V. Paquit, D. K. Felde, and B. Riemer, "Creating Small Gas Bubbles in Flowing Mercury Using Turbulence at an Orifice," in *ASME Fluids Engineering Division Summer Meeting*, 2010.

[5] M. Wendel, A. Abdou, and B. Riemer, "Choked-Flow Inlet Orifice Bubbler for Creating Small Bubbles in Mercury," in *ASME 2013 Fluids Engineering Division Summer Meeting*, 2013.

[6] H. Abe and K. Matsuuchi, "Microbubble Producing Device, Vortex Breaking Nozzle for Microbubble Producing Device, Spiral Flow Producing Blade Body for Microbubble Producing Device, Microbubble Producing Method, and Microbubble Applied Device," 2007.

[7] H. Abe, M. Kazuo, and M. Iidaka, "Micro-Bubble Generator, Vortexbreakdown Nozzle for Micro-Bubble Generator, Vaneswirler for Micro-Bubble Generator, Micro-Bubble Generating Method, and Micro-Bubble Applying Device," vol. 2, no. 12, 2011.

[8] C. Martínez-Bazán, J. L. Montañés, and J. C. Lasheras, "On the breakup of an air bubble injected into a fully developed turbulent flow. Part 1. Breakup frequency," *J. Fluid Mech.*, vol. 401, p. S0022112099006680, 1999.

[9] P. Bradshaw, "Effects of streamline curvature on turbulent flow," *Advis. Gr. Aerosp. Res. Dev.*, no. AG 169, pp. 633–659, 1973.

[10] H. Kogawa, T. Naoe, H. Kyotoh, K. Haga, H. Kinoshita, and M. Futakawa, "Development of microbubble generator for suppression of pressure waves in mercury target of spallation source," *J. Nucl. Sci. Technol.*, vol. 52, no. 12, pp. 1461–1469, 2015.

[11] H. Kogawa, T. Naoe, H. Kyotoh, K. Haga, H. Kinoshita, and M. Futakawa, "Development of microbubble generator for suppression of pressure waves in mercury target of spallation source," *J. Nucl. Sci. Technol.*, vol. 52, no. 12, pp. 1461–1469, 2015.

[12] C. A. Schneider, W. S. Rasband, and K. W. Eliceiri, "NIH Image to ImageJ: 25 years of image analysis," *Nature Methods*, vol. 9, no. 7. pp. 671–675, 2012.

[13] J. Canny, "A Computational Approach to Edge Detection," *IEEE Trans. Pattern Anal. Mach. Intell.*, vol. PAMI-8, no. 6, pp. 679–698, 1986.